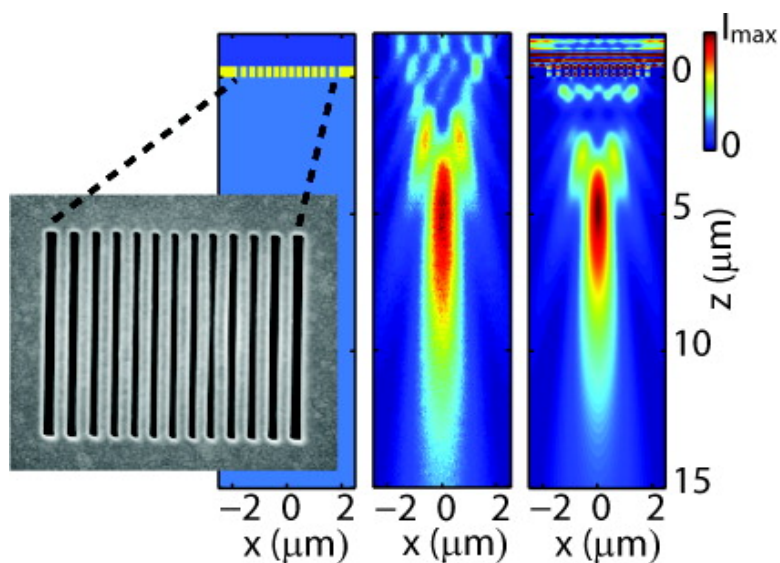


Planar Lenses Based on Nanoscale Slit Arrays in a Metallic Film

Lieven Verslegers, Peter B. Catrysse, Zongfu Yu, Justin S. White,
Edward S. Barnard, Mark L. Brongersma, and Shanhui Fan

Nano Lett., **2009**, 9 (1), 235-238 • DOI: 10.1021/nl802830y • Publication Date (Web): 21 November 2008

Downloaded from <http://pubs.acs.org> on January 21, 2009



More About This Article

Additional resources and features associated with this article are available within the HTML version:

- Supporting Information
- Access to high resolution figures
- Links to articles and content related to this article
- Copyright permission to reproduce figures and/or text from this article

[View the Full Text HTML](#)

Planar Lenses Based on Nanoscale Slit Arrays in a Metallic Film

Lieven Verslegers,^{†,§} Peter B. Catrysse,^{†,§,*} Zongfu Yu,[†] Justin S. White,[‡]
Edward S. Barnard,[‡] Mark L. Brongersma,[‡] and Shanhui Fan^{†,*}

*E. L. Ginzton Laboratory, Geballe Laboratory for Advanced Materials (GLAM),
Stanford University, Stanford, California 94305*

Received September 17, 2008; Revised Manuscript Received November 10, 2008

ABSTRACT

We experimentally demonstrate planar lenses based on nanoscale slit arrays in a metallic film. Our lens structures consist of optically thick gold films with micron-size arrays of closely spaced, nanoscale slits of varying widths milled using a focused ion beam. We find excellent agreement between electromagnetic simulations of the design and confocal measurements on manufactured structures. We provide guidelines for lens design and show how actual lens behavior deviates from simple theory.

With the advent of nanofabrication techniques, such as electron-beam lithography and focused ion beam milling, it has become possible to pattern metallic structures at the nanoscale. This has enabled the exploitation of the plasmonic behavior of metals to create new ultracompact photonic devices.^{1–3} In this context, we report here on the experimental demonstration of a novel plasmonic lens. Refractive lenses are some of the most ubiquitous optical components; they are widely used in applications that range from imaging to concentrating light. In fact, the miniaturization of lenses has been essential in the development of modern solid-state image sensors and can also have important implications for other opto-electronic applications such as displays, solid state lighting, and potentially solar cells. The focusing capability of conventional, dielectric-based microlenses however deteriorates as their physical dimensions are reduced toward a single-wavelength scale. Recently, nanopatterning of optically thick metallic films was theoretically proposed as an alternative to refractive lensing.^{4,5} The basic geometry consists of an array of nanoscale slits in an otherwise opaque metallic film (Figure 1a). For a plane wave incident upon such a structure, the phase shift experienced by light as it passes through each individual slit is sensitive to either the length,⁴ width,⁵ or even the materials inside the slit. With the adjustment of the properties of individual slits, it becomes possible to create a curved phase front for the transmitted field and thus to achieve a focusing action. None of the previous works report an experimental demonstration of far-

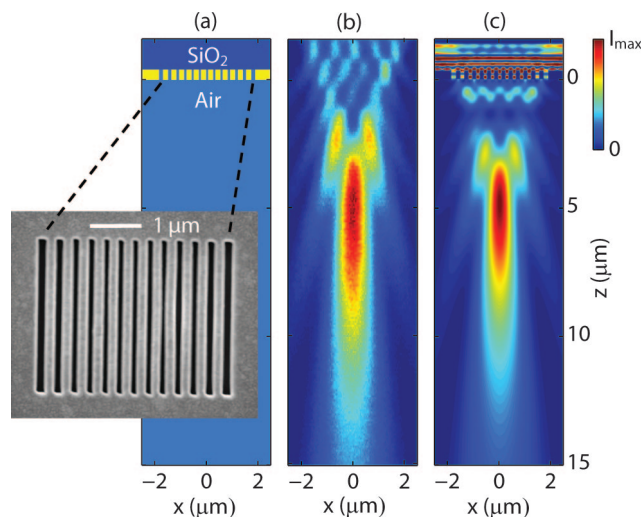


Figure 1. Planar lens based on nanoscale slit array in metallic film. (a) Geometry of the lens consisting of a 400 nm optically thick gold film (yellow) with air slits of different widths (80 to 150 nm) (light blue) milled therein on a fused silica substrate (dark blue). The inset shows a scanning electron micrograph of the structure as viewed from the air-side. (b) Focusing pattern measured by confocal scanning optical microscopy (CSOM). (c) Finite-difference frequency-domain (FDFD) simulated focusing pattern of the field intensity through the center of the slits. In order to show the features of the focus spot clearly, the field intensity inside the slits is saturated.

field lensing based on nanoslits. (We know that there has been recent experimental work based on nanoholes.^{6,7} It is known however that nanoslits exhibit higher transmission efficiency than nanoholes.⁸)

In this letter, we report the first experimental demonstration of far-field lensing using a plasmonic slit array. We implement a planar nanoslit lens using a combination of thin film

* To whom correspondence should be addressed. E-mail: (P.B.C.) pcatrys@stanford.edu; (S.F.) shanhui@stanford.edu.

[†] E. L. Ginzton Laboratory.

[‡] Geballe Laboratory for Advanced Materials (GLAM).

[§] These authors contributed equally to this work and should be considered joint first.

deposition and focused ion beam milling. We demonstrate experimentally that it acts as a far-field cylindrical lens for light at optical frequencies. We show excellent agreement between the full electromagnetic field simulations of the design, which include both evanescent and propagating modes, and the far-field, diffraction-limited confocal measurements. This first experimental demonstration is a crucial step in the realization of this potentially important technology, which offers a range of processing and integration advantages over conventional shaped-based dielectric lenses.

The fabricated planar lens structures consist of an array of nanoscale slits in a 400 nm, optically thick metal film. The slits range in width from 80 nm at the center of the array to 150 nm on the side, are spaced 200 nm apart, and are 3 μm long (Figure 1a). We fabricate the lenses in a two-step process. First, a metal film is evaporated onto a fused silica substrate using electron beam evaporation (pressure $<5 \times 10^{-7}$ Torr; deposition rate $\sim 2 \text{ \AA/s}$). For the metal film, we opt for gold because it does not oxidize and has a good plasmonic response in the visible part of the electromagnetic spectrum, that is, the phase can be sufficiently modulated by varying slit width while losses are moderate. Next, we nanopattern the gold films by milling through the film using an FEI Strata 235DB dual-beam focused ion beam (FIB) (10 pA Ga^+ ion beam current)/scanning electron microscope (SEM). All slits of the arrays are milled in parallel to prevent metal redeposition. The resulting lens structures are imaged by SEM (Figure 1a inset).

The structures are designed to operate as far-field lenses. Rather than using near-field scanning optical microscopy (NSOM), which requires a metallic probe in the vicinity of the lens and causes a perturbation of local fields, we use (far-field) confocal scanning optical microscopy (CSOM) to characterize the lens structures.⁹ In our experiments, we illuminate with a wide-area uniform beam and we use a Nikon 100 \times (NA 0.90) objective lens in a WITec alpha300 S confocal microscope to collect photons. A Sanyo 35 mW laser diode with measured emission at 637 nm is used to illuminate the sample through the fused silica. Laser light is polarized perpendicular to the long-axis of the slits. The laser beam is orders of magnitude wider than the lens structure so that it can be considered locally as a plane wave. Confocal scanning is done using a piezo-electrically driven 2-axis stage with subnanometer resolution in the x and y directions and a stepper motor with 60 nm resolution in the z direction. The focusing pattern (Figure 1b) is imaged in steps of 47 nm in the x direction and 78 nm in the z direction. This oversamples the intensity distribution and resolves all far-field features. A 25 μm multimode fiber acts as a pinhole in the confocal setup, offering a good empirical compromise between a small collection volume and large collection efficiency. A Hamamatsu 8259-01 photomultiplier tube is used to count photons collected over 2 ms integration time. The illumination intensity of the laser source is adjusted to remain in the linear range of the photon counting regime and integration time is chosen to achieve an SNR of more than 40:1 at the focus.

For a detailed analysis of the structure, we perform two-dimensional electromagnetic field simulations based on a finite-difference frequency-domain (FDFD) method.¹⁰ FDFD calculates the electromagnetic fields by solving a large sparse linear system derived from Maxwell's equations and allows us to model materials using tabulated experimental dielectric constants, including both real and imaginary parts, at every frequency. A plane wave with transverse magnetic (TM) polarization is used as a source. This plane wave excites the plasmonic waveguide modes in the slits upon incidence on the metallic structure. We set the grid size to 5 nm in the transverse x direction and 20 nm in the longitudinal z direction. This enables us to model the very fine features of the field at the metal–air interfaces inside the slits while maintaining a reasonable simulation domain size. The permittivity of gold and fused silica are set to $-11.04 + 0.78i$ and 2.13, respectively, at a wavelength of 637 nm.¹¹ We correct for the fact that the finite length of the slits causes diffraction in the y direction by doing an additional two-dimensional transverse electric (TE) simulation of an aperture with width equal to the slits length. TE and TM simulations are then combined, resulting in a “three-dimensional” field pattern.

Figure 1 shows the main results of the work, which combines fabrication, characterization, and simulation. Panel a shows the fabricated structure, while panels b and c represent the measured and simulated field intensity in a cross section through the center of the slits (along the x direction). Both the measurement and the simulation clearly demonstrate focusing of the wave. The agreement between experiment and simulation is excellent. Moreover, the simulation image is generated using the designed parameters as the slit width rather than the actual slit width measured in the SEM, as is commonly done when comparing nanophotonics simulation and experiments. The agreement here thus indicates the robustness in design and the fault tolerance of this approach for focusing.

Figure 2 allows for a more detailed quantitative discussion of the experimental and simulation results. Two cross sections through the focus spots of Figure 1b,c are shown: one in the x direction (Figure 2a) and one in the z direction (Figure 2b). The simulated field intensity distributions are in excellent agreement with the experimental distributions. The full width at half-maximum (fwhm) at focal point is 0.88 μm and the depth of focus is 6.23 μm in the simulated results. A small deviation from the simulation is expected in the measurements. Confocal microscopy collects light from a finite diffraction-limited volume; therefore the actual focusing pattern is convolved with this collection volume, causing features to appear somewhat broader. Since the features we are resolving are larger than the collection volume, this convolution modifies the result only slightly. Near to the film the collection volume moves into the film, making interpretation and comparison hard. Some uncertainty exists about the z -position of the gold surface in measurements. We therefore estimated its position in two ways: we measured the diffraction pattern of crosshairs (milled sufficiently far from the lens structures so that they do not

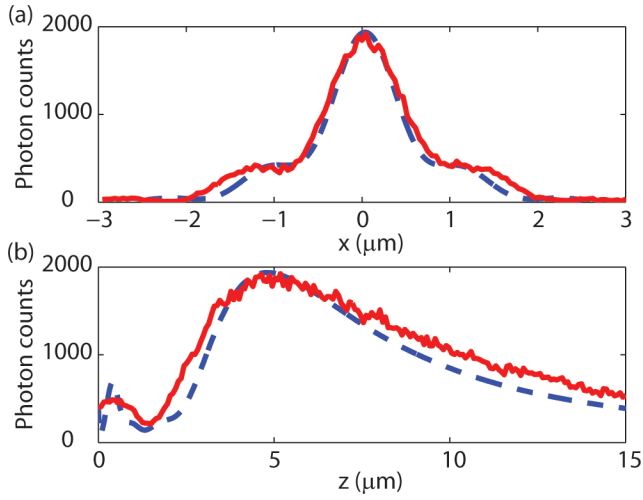


Figure 2. Focusing by a nanoscale slit array in a metallic film. FDFD simulated (dashed blue line) and CSOM measured (solid red line) photon counts (proportional to intensity) in cross sections of the focus along the x direction (a) and z direction (b).

interfere with the lenses), and we estimated the position of the film as the mirror plane of these patterns. Further matching of lens focusing patterns obtained in simulation and by measurement shows that this initial estimate is fairly accurate. We checked the polarization dependence of the devices. For light polarized parallel to the slits, no focusing is observed due to the absence of propagating modes in the slits. We also note the onset of side lobes in Figure 2a, which is a result of the limited size of the lens. The small amount of noise in the measurements can be understood mainly as shot noise and to a lesser extent as dark counts.

We now discuss in more detail the underlying physics involved in designing these planar lenses. We start with the simple intuitive picture that has been proposed for the design.⁵ The basic building block of the patterned metallic lens is a narrow slit surrounded by metallic walls. The transverse magnetic (TM) mode of this metal-insulator-metal (MIM) structure follows the dispersion relationship¹²

$$\tanh\left(\sqrt{\beta^2 - k_0^2} \frac{w}{2}\right) = \frac{-\sqrt{\beta^2 - k_0^2} \epsilon_m}{\epsilon_m \sqrt{\beta^2 - k_0^2}} \quad (1)$$

which links the waveguide propagation constant β to the free space propagation constant k_0 , the permittivity of the metal ϵ_m and the slit width w . A single-pass phase delay introduced by a slit is βd with d being the film thickness. This phase delay strongly depends on slit width as can be seen from Figure 3a. For a narrower slit, a larger portion of the mode resides in the metal and therefore light travels slower. Thus, a narrow slit introduces more phase delay. This explains how a structure consisting of slits with width increasing from the center to the side (inset of Figure 3b) creates a curved wavefront.

The phase front curvature, as generated by the single pass phase delay through individual slits, is not sufficient to account for all the physics occurring in our experimental planar lens. For the waves of individual slits to be in phase at the focal distance f from the lens, the phase delay as a

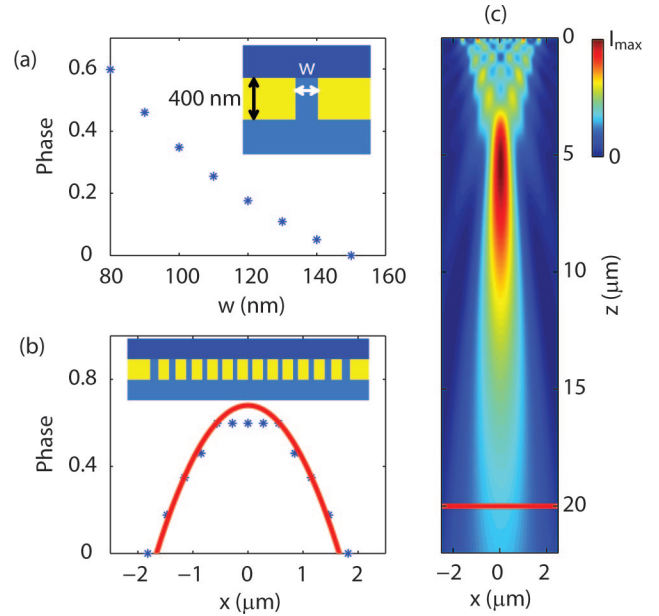


Figure 3. Design of a nanoscale slit array to achieve optical lens functionality. (a) phase delay introduced by a 400 nm deep slit as a function of slit width w . (b) The slit array (inset) builds up a phase front (blue dots) that mimics that of a cylindrical wave (red line). (c) 2D FDFD simulated focusing pattern of the magnetic field intensity of the lens. The red line indicates the predicted focal length based on a geometrical argument presented in eq 2.

function of distance x from the center of the lens, as predicted from a geometrical argument, has to be

$$\varphi(x) = 2n\pi + \frac{2\pi f}{\lambda} - \frac{2\pi\sqrt{f^2 + x^2}}{\lambda} \quad (2)$$

with λ as the wavelength and n as an arbitrary integer. For our choice of slit widths and spacing, eq 2 (the red curve in Figure 3b) predicts a focal length of approximately 20 μm . The location of the focal length design value is indicated (red line) on the FDFD simulation of the actual structure in Figure 3c. This simulation is two-dimensional, corresponding to infinitely long slits. This shows that the intuitive geometrical theory does not predict the actual focal length (5.3 μm) quantitatively. The actual focal length is to a large degree determined by the lens size.¹³ The discrepancy between simple theory and the full-field simulations and measurements stems mainly from this effect. The phase delay will also deviate from βd , because light can go through Fabry–Pérot oscillations in the slit, leading to an additional phase contribution and an expected shorter focal length. Moreover, the transmission of individual slits varies as a function of slit width, leading to amplitude modulation of the field at the exit surface of the film. This amplitude modulation effect does not work to our advantage here, since the wider slits near the side of the lens typically transmit more light. In general, one would want more light near the center of the lens to counteract diffraction. Fortunately, all these deviations from the simple geometrical theory can be accounted for in the FDFD simulations used in our design with excellent agreement between the full-field simulations and experiments.

In fact, the effect of lens size can be exploited to control the focusing behavior as is shown clearly in Figure 4. Both lenses introduce the same curvature to the incident plane

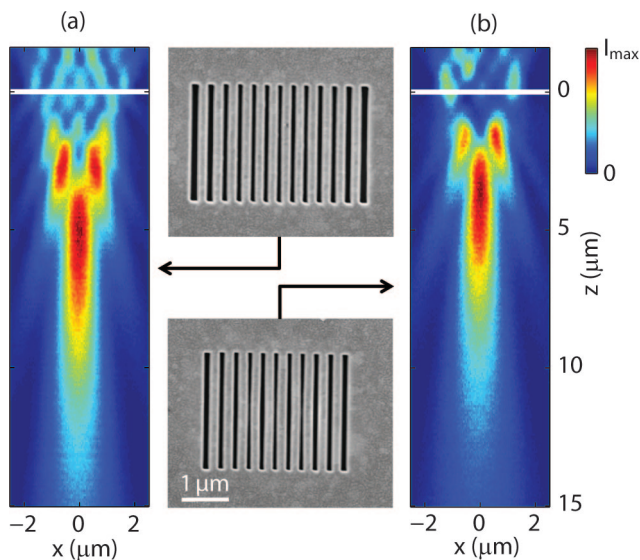


Figure 4. Control of the cylindrical lens behavior by design of nanoscale slit array parameters. Effect of lens size on focusing for (a) a lens with 13 slits (80–150 nm by $2.5\ \mu\text{m}$) and (b) a lens with 11 slits (80–120 nm by $2.5\ \mu\text{m}$). The white line gives an estimate of the lens position. Both scanning electron micrographs are on the same scale.

wave as the lens from Figure 1, since they consist of slits with the same width as the original design ($2.5\ \mu\text{m}$ long). By omitting one outer slit on each side for the lens in Figure 4a, one gets the lens in Figure 4b. Even though these structures have the same phase front curvature, the actual focus moves closer to the gold film as the lenses get smaller, in good agreement to what our simulations predict. This confirms that, as lenses are scaled down to the size of only a couple of wavelengths and especially for long focal lengths, the simple eq 2 is no longer valid and merely provides an approximate starting point. A similar effect shows up for lenses that only differ in slit length: lenses with short slits cannot achieve a focus far from the lens.

As a final remark, we comment on the design rules for the slit lens. In the devices considered here, the spacing between individual slits is much larger than the skin depth. As a result, slits are not coupled. The dependency of the device characteristics on the slit spacing is therefore fairly weak. In this weak coupling regime, the MIM dispersion relationship of an individual slit can be used as a starting point to derive the phase front curvature used for lens design, as has been commonly done in the literature. Our results here indicated however that the corresponding focal length estimate needs to be corrected for various factors, most notably the finite aperture size and to a lesser degree Fabry–Pérot oscillations and amplitude modulation as light

is transmitted through individual slits. The impact of these effects can only be accurately determined through numerical simulation. The general trend is that they tend to lead to a shorter focal length. In the opposite regime, which we have not explored experimentally, when the gold spacing between the slits is comparable to or smaller than the skin depth, the independent slit approximation is no longer valid. In such a case, since each slit is surrounded by less metal, the actual phase front curvature tends to be smaller than the estimate from the independent slit approximation, resulting in a correction toward a longer focal length.

In conclusion, we have shown experimental evidence of light focusing by nanopatterned optically thick gold films. We found our first-principles electromagnetic simulations and our confocal measurements to be in excellent agreement. We have pointed out limitations in previously established simple design rules and shown how lens size plays a crucial role when focusing light at the nanoscale. This first experimental demonstration is a crucial step in the realization of this potentially important technology for many applications in optoelectronics. Moreover, the design principles presented here for the specific case of a lens can be applied to construct a wide range of optical components that rely on tailoring of the optical phase front.

Acknowledgment. The authors acknowledge A. Kinkhabwala and Dr. W. E. Moerner for help in establishing that CSOM is a suitable characterization method and Dr. Y. Ono and Dr. D. J. Tweet for helpful discussions. This work was supported by Sharp Laboratories of America. J.W. and E.B. acknowledge the support of the Global Climate and Energy Project at Stanford University.

References

- (1) Engheta, N. *Science* **2007**, *317*, 1698–1702.
- (2) Shalaev, V. M. *Nat. Photonics* **2007**, *1*, 41–48.
- (3) Lal, S.; Link, S.; Halas, N. J. *Nat. Photonics* **2007**, *1*, 641–648.
- (4) Sun, Z.; Kim, H. K. *Appl. Phys. Lett.* **2004**, *85*, 642–644.
- (5) Shi, H.; Wang, C.; Du, C.; Luo, X.; Dong, X.; Gao, H. *Opt. Express* **2005**, *13*, 6815–6820.
- (6) Huang, F. M.; Kao, T. S.; Fedotov, V. A.; Chen, Y.; Zheludev, N. I. *Nano Lett.* **2008**, *8*, 2469–2472.
- (7) Huang, F. M.; Zheludev, N. I.; Chen, Y.; Garcia de Abajo, F. J. *Appl. Phys. Lett.* **2007**, *90*, 091119.
- (8) Garcia-Vidal, F. J.; Martin-Moreno, L. *Phys. Rev. B* **2002**, *66*, 155412.
- (9) Corle, T. R.; Kino, G. S. *Confocal Scanning Optical Microscopy and Related Imaging Systems*, 1st ed.; Academic Press: San Diego, 1996.
- (10) Veronis, G.; Fan, S. Overview of Simulation Techniques for Plasmonic Devices. In *Surface Plasmon Nanophotonics*; Brongersma, M. L., Kik, P. G., Eds.; Springer: New York, 2007; Vol. 131, pp 169–182.
- (11) *CRC Handbook of Chemistry and Physics*, 88th ed.; Lide, D. R., Ed.; CRC Press: Boca Raton, FL, 2003.
- (12) Economou, E. N. *Phys. Rev.* **1969**, *182*, 539–554.
- (13) Ruffieux, P.; Scharf, T.; Herzig, H. P.; Völkel, R.; Weible, K. J. *Opt. Express* **2006**, *14*, 4687–4694.

NL802830Y